Fast clear-sky solar irradiation computation
for very large digital elevation models

L.F. Romero [a,1], Siham Tabik [a,*,1], Jesús M. Vías [b], Emilio L. Zapata [a]

[a] *Department of Computer Architecture, University of Málaga, 29071 Málaga, Spain*
[b] *Department of Geography, University of Málaga, 29071 Málaga, Spain*

Abstract

This paper presents a fast algorithm to compute the global clear-sky *irradiation*, appropriate for extended high-resolution Digital Elevation Models (DEMs). The latest equations published in the European Solar Radiation Atlas (ESRA) have been used as a starting point for the proposed model and solved using a numerical method. A new calculation reordering has been performed to (1) substantially diminish the computational requirements, and (2) to reduce dependence on both, the DEM size and the simulated period, i.e., the period during which the *irradiation* is calculated. All relevant parameters related to shadowing, atmospheric, and climatological factors have been considered. The computational results demonstrate that the obtained implementation is faster by many orders of magnitude than all existing advanced *irradiation* models while maintaining accuracy. Although this paper focuses on the clear-sky *irradiation*, the developed software also computes the global *irradiation* applying a filter that considers the clear-sky index.

1. Introduction

Knowledge of the amount of incoming solar *irradiation* at different geographic locations is of paramount importance in diverse fields such as solar energy utilization, building design, agriculture, remote sensing, environmental assessment and ecology.
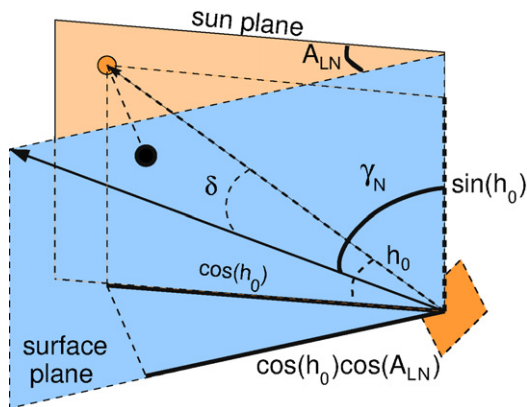
The development of *irradiation* models has progressed significantly in the last two decades [1]. Solar Analyst [2], developed under ArcView GIS, calculates the hemispherical viewshed for each cell of the DEM; it then generates sun-maps and sky-maps to rapidly calculate direct and diffuse radiation. This model is appropriate enough for the study of solar *irradiation* in small DEMs (i.e., of the order of thousands of points) and for small periods but it is rather limited for larger areas. SRAD [3], also developed under ArcView GIS, is based on a simplified

representation of the underlined physics, able to characterize the spatial variability of the landscape processes; however, its application over large terrains is also limited. The r.sun model [4] implemented under GRASS GIS 6.2.2 environment [5], is based on the European Solar Radiation Atlas (ESRA) equations [6,10], solved numerically. Despite of the fact that this software is the fastest of all the existing models, it is only applicable for medium-scale areas because of its very high computational cost; at least five times more expensive when terrain shadowing (also called horizon) computation is included. Moreover, the *irradiation* computation *per se* is costly and becomes more expensive or even unapproachable as the DEM size and resolution increase and/or the simulated period is longer, since the *irradiation* is re-calculated for each DEM cell and each time-step.

The aim of this work is to introduce an alternative integration method together with a domain discretization to calculate the *irradiation* for a reduced number of points and then to reuse these calculations for points that have identical characteristics. A large part of the calculation can be substantially reduced by searching for equivalences until reducing it the smallest mini-

---

* Corresponding author. Tel.: +34 952 13 41 69; fax: +34 952 13 27 90.
  E-mail address: siham@ac.uma.es (S. Tabik).
[1] Both authors contributed equally to this work.

Fig. 1. Geometrical formulation of the solar incidence angle δ.

mum possible. In particular, this paper presents a fast algorithm that reduces the dependence of calculation on both terrain size and simulated period. This model is appropriate for the estimation of clear-sky *irradiation* on very large terrains, i.e., high resolution DEMs of the order of millions of cells. Parallel computing has also been introduced into the code to benefit from current computational systems such as those based on multicore (e.g., duo-core) processors and shared memory computers.

This paper is organized as follows: the mathematical expressions that represent the physics of the phenomenon along with a detailed study of dependencies are provided in Section 2. In addition to a description of the main stages of the numerical integration, a comparison between our model and ESRA model is given in Section 3. Both a computational analysis and a comparative study in terms of numerical and runtimes results between r.sun and the proposed model have been carried out in Section 4. Finally, conclusions are given in Section 5.

2. Mathematical formulation

The calculation of the instantaneous, global, solar *irradiance* (W m^{-2}) under a clear-sky on a given terrain depends on the sun position (its altitude, h_0, and azimuth, A_0), the atmospheric attenuation, represented by the Linke turbidity factor, T_{LK}, and the characteristics of the considered point of the DEM or surface, i.e., its inclination angle (also called slope), γ_N, azimuth (also called aspect), A_N (i.e., the angle between the projection of the normal on the horizontal surface and the north), elevation, z, and self- and terrain shadowing effect. The global *irradiance*, G_{ic}, under clear-sky (i.e., cloudless atmosphere) on an inclined plane can be expressed as the sum of its beam, B_{ic}, diffuse, D_{ic}, and reflected, R_{ic}, components:

$$G_{ic} = B_{ic} + D_{ic} + R_{ic}. \tag{1}$$

The beam *irradiance* is calculated as:

$$B_{ic} = I_0 \cdot \varepsilon \cdot I_{\text{direct}}, \tag{2}$$

where

$$I_{\text{direct}} = K_b \cdot \cos(\delta).$$

ε is a correction factor that allows for a varying solar distance. K_b, is the proportion between *irradiance* and extraterrestrial

solar *irradiance* on a horizontal surface, and depends on h_0, the Linke turbidity factor T_{LK} and the height of the considered surface z; δ is the solar incidence angle measured between the sun and the inclined surface; as illustrated in Fig. 1, $\cos(\delta)$ can be formulated as:

$$\cos(\delta) = \cos(\gamma_N) \cdot \sin(h_0)$$
$$+ \sin(\gamma_N) \cdot \cos(h_0) \cdot \cos(A_{LN}). \tag{3}$$

The diffuse *irradiance* is calculated as:

$$D_{ic} = I_0 \cdot \varepsilon \cdot F_1 \cdot I_{\text{diffuse}}, \tag{4}$$

where

$$F_1 = T_n(T_{LK}) \cdot F_d(h_0).$$

T_n is a diffuse transmission function that depends only on T_{LK} and F_d is the diffuse solar altitude function which depends only on the solar altitude h_0 [6].

The model adopted by ESRA for clear-sky diffuse *irradiance* on an inclined surface, initially proposed by Muneer [7], distinguishes between sunlit and shadowed surfaces. For sunlit surfaces, i.e., $h_0 \geqslant hor$, where hor is the horizon angle in degree, the *irradiance* is calculated using two terms: the first depends on both the sun position and the surface inclination angle, and the second depends only on the sun elevation in the sky. Therefore, the diffuse *irradiance*, I_{diffuse}, can be reordered as the sum of three components: radiation in shadow, I_i, sun elevation-dependent radiation, I_{ii}, and sun position-dependent radiation, I_{iii} (i.e., circumsolar radiation). The three terms can be written as follows:

$$I_i = F(\gamma_N) \quad \text{if } 0 \leqslant h_0 < hor,$$

$$I_{ii} = (1 - K_b) \cdot F(\gamma_N) \quad \text{if } h_0 \geqslant hor$$

$$I_{iii} = \begin{cases} I'_{iii} = K_b \cdot \frac{\cos(\delta)}{\sin(h_0)} & \text{if } h_0 \geqslant 5.7° \text{ and } h_0 \geqslant hor, \\ I''_{iii} = K_b \cdot \frac{\sin(\gamma_N) \cdot \cos(A_{LN})}{0.1 - 0.008 h_0} & \text{if } hor \leqslant h_0 < 5.7°, \end{cases}$$

where

$$F(\gamma_N) = r(\gamma_N)$$
$$+ \left(\sin(\gamma_N) - \gamma_N \cdot \cos(\gamma_N) - \pi \cdot \sin^2(\gamma_N/2)\right) \cdot N,$$

$$r(\gamma_N) = \frac{1 + \cos(\gamma_N)}{2},$$

$$N = \begin{cases} 0.00263 - 0.712 \cdot K_b - 0.6883 \cdot K_b^2 \\ \qquad \text{for sunlit surfaces } (h_0 \geqslant hor), \\ 0.25227 \quad \text{surfaces in shadow } (h_0 < hor), \end{cases}$$

$$A_{LN} = A_0 - A_N.$$

As shown above, the formulation of $F(\gamma_N)$ varies if the sun is above or below the horizon and the component I_{iii} is different during sunset and sunrise. Introducing the following boolean coefficients λ_{shad} (1 if the sun is below the horizon $h_0 \geqslant hor$, 0 otherwise) and λ_{twi} (1 if the sun elevation is smaller than 5.7°, 0 otherwise), G_{ic} can be rewritten as follows:

$$G_{ic} = I_0 \cdot \varepsilon \cdot \left[(1 - \lambda_{\text{shad}}) \cdot K_b \cdot \cos(\delta) \cdot \left\{ 1 + \frac{F_1 \cdot (1 - \lambda_{twi})}{\sin(h_0)} \right\} \right.$$
$$\left. + F_1 \cdot \{I_i + I_{ii} + I_{iii}''\} \right] + R_{ic}, \tag{5}$$

where

$$I_i = \lambda_{\text{shad}} \cdot I_i = \lambda_{\text{shad}} \cdot F(\gamma_N, \lambda_{\text{shad}}),$$
$$I_{ii} = (1 - \lambda_{\text{shad}}) \cdot I_{ii} = (1 - \lambda_{\text{shad}}) \cdot (1 - K_b) \cdot F(\gamma_N, \lambda_{\text{shad}}),$$
$$I_{iii}'' = (1 - \lambda_{\text{shad}}) \cdot \lambda_{twi} \cdot I_{iii}''$$
$$= (1 - \lambda_{\text{shad}}) \cdot \lambda_{twi} \cdot K_b \cdot \frac{\sin(\gamma_N) \cdot \cos(A_{LN})}{0.1 - 0.008 h_0}.$$

Note that both direct *irradiance* and circumsolar fraction of the diffuse *irradiance* depends on δ.

The ground reflected clear-sky *irradiance* received on an inclined surface, R_c, is proportional to the global horizontal *irradiance*, G_{hc}, the mean ground albedo, ρ_g, and the fraction of the ground viewed by the inclined surface, $r_g(\gamma_N)$ [8]:

$$R_c = \rho_g \cdot G_{hc} \cdot r_g(\gamma_N). \tag{6}$$

Notice that the global *irradiance* on horizontal planes, G_{hc}, can be calculated from Eq. (5) by replacing the inclination angle of the surface γ_N by 0. Therefore, a natural way of calculation is to first calculate the quantity:

$$B_{ic} + D_{ic}$$
$$= I_0 \cdot \varepsilon \cdot \left[(1 - \lambda_{\text{shad}}) \cdot \cos(\delta) \cdot \left\{ 1 + \frac{F_1 \cdot (1 - \lambda_{twi})}{\sin(h_0)} \right\} \right.$$
$$\left. + F_1 \cdot \{I_i + I_{ii} + I_{iii}''\} \right] \tag{7}$$

then the reflected *irradiance*, R_{ic}, can be calculated using $G_{hc} = B_{hc} + D_{hc}$ ($\gamma_N = 0$) and finally the global clear-sky *irradiance* on inclined planes, G_{ic}, can be straightforwardly obtained.

3. Numerical integration

The global clear-sky *irradiation* (W h m^{-2}) in a given time-interval is calculated by the integration of the instantaneous *irradiance* (W m^{-2}) in time [6,9,10]. This integration can be performed analytically or numerically. ESRA [6] offers two robust models based on two different formulations of the problem. The first model is only employed for computing the *irradiance*, while the second computes the *irradiation* by analytically integrating an alternative empirical formulation of the *irradiance*. Rigollier [10] has shown that both methods give similar results of *irradiance*, but the second is best suited for the *irradiation* because the analytical integration provides better accuracy under irregular shadowing conditions. However, in this work, we have used a new integration method of the first equations to compute *irradiation*. In particular, we have employed a numerical method that: (1) optimizes the calculation using a new ordering in time and space; and (2) allows a very accurate *irradiance* calculation and numerical integration of *irradiation*, even under irregular shadowing, by employing very small time-steps. The sun takes four minutes to travel a distance of one

degree. Therefore, four minutes is the minimum value of time-step necessary to provide a very accurate calculation. However, in this work we have used a smaller time-step, of one minute, to provide even more accurate results, especially for the calculation of sunrise and sunset times if precise horizon data are available.

In other words, we have computed the *irradiation* as a sum of the discrete values of *irradiance* at each single time-step in the time-interval $[t_{\text{ini}}, t_{\text{end}}]$, where t_{ini} and t_{end} are respectively the start and end time of the simulation period, thus, the integration of Eq. (7) in time can be expressed as follows:

$$B_{ic} + D_{ic}$$
$$= I_0 \cdot \sum_{t_{\text{ini}}}^{t_{\text{end}}} \left\{ (1 - \lambda_{\text{shad}}) \cdot \cos(\delta) \cdot \left(1 + \frac{F_1 \cdot (1 - \lambda_{twi})}{\sin(h_0)} \right) \right.$$
$$\left. + F_1 \cdot I_i + F_1 \cdot I_{ii} + F_1 \cdot I_{iii}'' \right\} \cdot \varepsilon \cdot \Delta t. \tag{8}$$

The main stages of the employed numerical method are described in detail in the next subsections.

3.1. Sky discretization

The first simplification consists of constructing a sky-map of hemispherical shape that covers the considered surface. Since $0 \leqslant h_0 \leqslant 90°$ and $0 \leqslant A_0 \leqslant 360°$, we have discretized this map into $N_s = N_{h_0} \times N_{A_0}$ windows along the angular coordinates, altitude and azimuth. The discretization error should be small enough to be negligible compared to the atmospheric variability which is the dominant error in any solar irradiation model. Expression (8) can be evaluated by grouping its terms in each window each time the sun is in that position of the sky. For a discretization of $N_s = 90 \times 360$ windows, with 1×1 degree angle-step, $B_{ic} + D_{ic}$ can be rewritten as:

$$B_{ic} + D_{ic} = I_0 \cdot \Delta t \cdot \sum_{A_0=0}^{360°} \sum_{h_0=0}^{90°} \sum_{m=m_{\text{ini}}}^{m_{\text{end}}} \left[\sum_{k=1}^{k=n_{h,A_0}} \left\{ I_d \cdot \cos(\delta) \right. \right.$$
$$\left. \cdot \left(1 + \frac{F_1 \cdot (1 - \lambda_{twi})}{\sin(h_0)} \right) \right.$$
$$\left. \left. + F_1 \cdot I_i + F_1 \cdot I_{ii} + F_1 \cdot I_{iii}'' \right\} \right] \cdot \varepsilon, \tag{9}$$

where n_{h,A_0} is the number of times the sun has passed through the window of angular coordinates (h, A_0) in the time-interval $[t_{\text{ini}}, t_{\text{end}}]$, with $0 \leqslant h \leqslant 90°$; $\lambda_{twi} = f(h_0)$, $F_1 = f(h_0, m, z)$, $K_b = f(h_0, m, z)$ and $n_{h,A_0} = f(h_0, A_0, m)$; m is the month number (with $0 \leqslant m \leqslant 12$), being m_{ini} and m_{end} the first and last months of the simulation, respectively. Although expression (9) should be computed for all points of the terrain, the proposed sky-map allows us to reuse calculations for surfaces with the same orientation and height. We have grouped the five terms of Eq. (9) by months, since the extracted climatological parameters from SoDa database, such as the Linke turbidity factor, T_{LK}, are only available in monthly averages, and their interpolation is also obtained in monthly values. To ease calculation even more, we have re-classified the five terms into five

components although this classification does not correspond to the traditionally physical one. Therefore, our model can only use monthly averages of the Linke turbidity factor. However, this fact does not affect the simulation period that could be on the order of minutes, days, weeks, months, or years. Nevertheless, in the future, if new daily or hourly averages of the climatological parameters are available, they can be easily included in our model. Replacing $\cos(\delta)$ by Eq. (3) in Eq. (9) we obtain:

$$B_{ic} + D_{ic} = I_0 \cdot \Delta t$$
$$\cdot \sum_{A_0=0}^{360°} \left\{ (1 - \lambda_{\text{shad}}) \cdot (T_1 + T_2) + T_3 + T_4 + T_5 \right\}, \tag{10}$$

where

$$T_1 = \cos(\gamma_N) \cdot \sum_{h_0=hor}^{90°} \sum_{m=m_i}^{m_e} \sin(h_0) \cdot K_b$$
$$\cdot \left(1 + \frac{F_1 \cdot (1 - \lambda_{twi})}{\sin(h_0)} \right) \cdot \sum_{k=1}^{n_{h,A_0}} \varepsilon,$$

$$T_2 = \cos(A_{LN}) \cdot \sin(\gamma_N) \cdot \sum_{h_0=hor}^{90°} \sum_{m=m_i}^{m_e} \cos(h_0) \cdot K_b$$
$$\cdot \left(1 + \frac{F_1 \cdot (1 - \lambda_{twi})}{\sin(h_0)} \right) \cdot \sum_{k=1}^{n_{h,A_0}} \varepsilon,$$

$$T_3 = F(\gamma_N, 1) \cdot \sum_{h_0=0}^{hor} F_d(h_0) \sum_{m=m_i}^{m_e} T_n(m) \cdot \sum_{k=1}^{n_{h,A_0}} \varepsilon,$$

$$T_4 = \sum_{h_0=hor}^{90°} \cdot \sum_{m=m_{\text{ini}}}^{m_{\text{end}}} F(\gamma_N, 0) \cdot F_1 \cdot (1 - k_b) \cdot \sum_{k=1}^{n_{h,A_0}} \varepsilon,$$

$$T_5 = \sin(\gamma_N) \cdot \cos(A_{LN}) \cdot \sum_{h_0=hor}^{5.7} \sum_{m=m_i}^{m_e} \frac{F_1 \cdot K_b}{0.1 - 0.008 \cdot h_0} \cdot \sum_{k=1}^{n_{h,A_0}} \varepsilon.$$

The terms, T_1, T_2, T_3, T_4 and T_5 have been calculated in three preprocessing stages as described in the next three subsections.

3.2. Stage 1: Sun trajectory calculation

First in this stage, the sun trajectory has been calculated without using any terrain data. Then, the matrix, $n = n(h_0, A_0, m) = \sum_{k=1}^{k=n_{h_0,A_0}} \varepsilon$, has been computed, where each of its elements stores the *extraterrestrial energy* received from the corresponding window of the sky, classified by month in the simulated period. For a simulated period of less than one month within the same month (e.g., one day), only the data of the corresponding month are used. This phase can be completed in about 0.45 seconds for a simulation time-interval of one year on a T2400 Intel Centrino duo processor. This is the only stage that depends on the simulated time-interval. For large territories, the computed sun trajectory can be shared by zones of similar latitude.

3.3. Stage 2: Height discretization

Given that the atmosphere parameters depend on the heights of the terrain, an analysis of the variation of global *irradiation* in terms of the height z has been carried out using experimental measurements available in SODA [12]. This study has proven that the dependency on the atmosphere parameters is not strong and changes in the atmosphere are completely negligible a few hundred meters above or below a given site. Hence, a height-step of 200 meters has been used in our model since the induced discretization error is of the same order as the one due to the $1° \times 1°$ sky discretization, as it has been experimentally tested. In this stage, the following matrices have to be filled:

$$M_1(z, A_0, h_0) = \sum_{m=m_{\text{ini}}}^{m_{\text{end}}} n \cdot \sin(h_0) \cdot K_b \cdot \left(1 + \frac{F_1 \cdot (1 - \lambda_{twi})}{\sin(h_0)} \right),$$

$$M_2(z, A_0, h_0) = \sum_{m=m_{\text{ini}}}^{m_{\text{end}}} n \cdot \cos(h_0) \cdot K_b \cdot \left(1 + \frac{F_1 \cdot (1 - \lambda_{twi})}{\sin(h_0)} \right),$$

$$M_3(z, A_0, h_0) = F_d(h_0) \cdot \sum_{m=m_{\text{ini}}}^{m_{\text{end}}} n \cdot T_n(m),$$

$$M_4(z, A_0, h_0, m) = n \cdot F_1 \cdot (1 - k_b),$$

$$M_5(z, A_0, h_0) = n \cdot \frac{F_1 \cdot K_b}{0.1 - 0.008 \cdot h_0}.$$

As the data structures, M_1, M_2, M_3, M_4 and M_5, depend on z, they can be calculated for all possible values of the discretized height (e.g., from 0 to 1000 m with a height-step $\Delta z = 200$ m), which would also make this phase completely independent on the terrain. However, if the terrain is known at this stage, the calculation can be restricted to the terrain altitude limits, z_{min} and z_{max}.

Once the atmospherical conditions are taken into account, the resulting matrices (i.e., the five classified terms) store the energies received from each window of the sky dome. A graphical representation of the term M_1 for a given point of the terrain is shown in Fig. 2. It should be noticed that this preprocessing stage can be performed at the same time as the first stage; that is, the energy terms can be classified while sun positions are computed. This fact would increase the numerical precision as $\sin(h_0)$ and $\cos(h_0)$ can directly use the computed values for the sun instead of the discretized values of the sky-map. However, it has two disadvantages: (1) it produces a loss in spatial locality of the code, and (2) it increases the fraction of the code that depends on the simulated period. Nevertheless, the computation in this phase takes only about 0.05 seconds per z-plane for a simulation of one year.

3.4. Stage 3: Horizon and slope discretization

At this stage, the horizon height, *hor*, must be already calculated using an appropriate algorithm. In this work, we have used a parallel horizon algorithm, which is an adaptation of Stewart's algorithm [15] for regular grids. The used algorithm not only computes both the shadowing produced by the cell itself (i.e., ground shadowing) and the one produced by all the cells
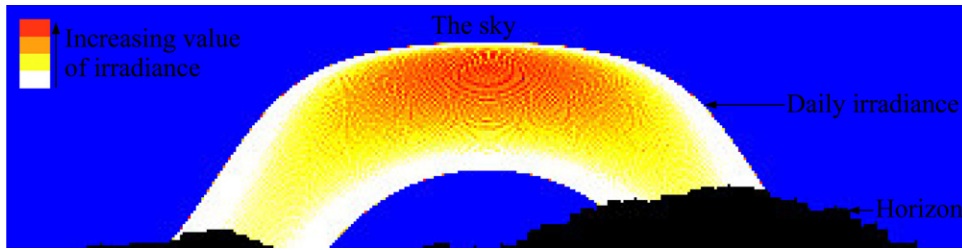
Fig. 2. The arc shape shows the component M_1 of the daily irradiance values tracking the position of the sun (A_0 represented in X-axis and h_0 represented in Y-axis) throughout the year, at a given point of the terrain. The black shape represents the horizon from the left to the right, in the north, east, south and west.
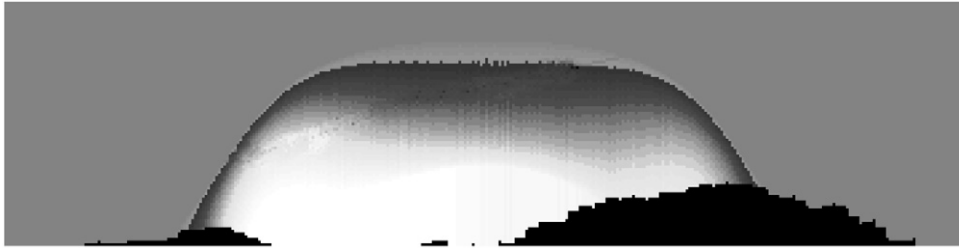

Fig. 3. Graphical representation of the term N_1, computed by integrating in altitude the term M_1 from hor to the zenith and by tracking the position of the sun (A_0 represented in X-axis and h_0 represented in Y-axis) throughout the year, at the same point as in Fig. 2.

that surround it [14], but also partitions the considered DEM in subgrids (or tiles) of size 1000×1000 cells so that each processor computes the horizon in its local subgrid using a multilevel halo to eliminate the edge effect associated with Stewart's algorithm, consider [14] for more details. In this preprocessing stage, the following structures have been calculated:

$$N_1(z, A_0, hor) = \sum_{h_0=hor}^{90°} M_1(z, A_0, h_0),$$

$$N_2(z, A_0, hor) = \sum_{h_0=hor}^{90°} M_2(z, A_0, h_0),$$

$$N_3(A_0, hor) = F_d(h_0) \cdot \sum_{h_0=0}^{hor} M_3(A_0, h_0)m,$$

$$N_4(z, \gamma_N, A_0, hor)$$
$$= \sum_{h_0=hor}^{90°} F(\gamma_N, 0) \cdot \sum_{m=m_{ini}}^{m_{end}} M_4(z, A_0, h_0, m), \quad \forall \gamma_N,$$

$$N_5(z, A_0, hor) = \sum_{h_0=hor}^{5.7} M_5(z, A_0, h_0).$$

These arrays have been computed for all possible values of hor, A_0, γ_N and z. Therefore, for each kind of irradiation and for each A_0, N_1, N_2, N_3, N_4 and N_5 store the sum of all the energy received from the window (hor, A_0) to the zenith. They actually store the first results of the spatial discretization of the sky dome. A graphical representation of term N_1, computed from the array M_1 of Fig. 2, is shown in Fig. 3.

The execution time of this stage depends only on the precision of the sky dome windows, the tilt, and the height limits z_{min} and z_{max} of the terrain; thus, they should be carefully dimen-

sioned so that N_1, N_2, N_3, N_4 and N_5 can be held in most main memories. Notice that z-dimension depends on the height-step and -limits while the rest of array dimensions are independent of terrain dimensions which ensures a computation with limited memory requirements. For an altitude and azimuth precision of one degree, typical execution times of this phase take about 4 seconds, and the memory usage is about 12 MB per z-plane. Due to the (relatively) high computational requirements of this stage, it should be performed when height limits are known. Partitioning the DEM of Andalusia, of surface 100000 km^2 [13], into tiles of 10×10 km^2, if the precision in altitude or azimuth is reduced to 2 or 4 degrees, both memory usage and runtime are reduced to the same factor and the final results only change slightly (typical deviations are around 2 to 7 J/m^2 in one year).

3.5. Clear-sky irradiation

Finally, the proposed *irradiation* algorithm integrates in azimuth by introducing the terrain data (i.e., heads and tilts of all points, and their corresponding horizon heights in all azimuthal directions) as follows:

```
For x = 0, grid x − 1
  For y = 0, grid y − 1
  /*Notice that A_N and γ_N are known at this stage*/
    For A_0 = 0, 360° − 1°
      val1+ = N_1(z, A_0, hor)
      val2+ = N_2(z, A_0, hor) · cos(A_LN)
      val3+ = N_3(A_0, hor)
      val4+ = N_4(z, γ_N, A_0, hor)
      val5+ = N_5(z, A_0, hor) · cos(A_LN)
      val6+ = hor/90
    End For
      G_hc = val1 + val3 · F(γ_N) + val4
```
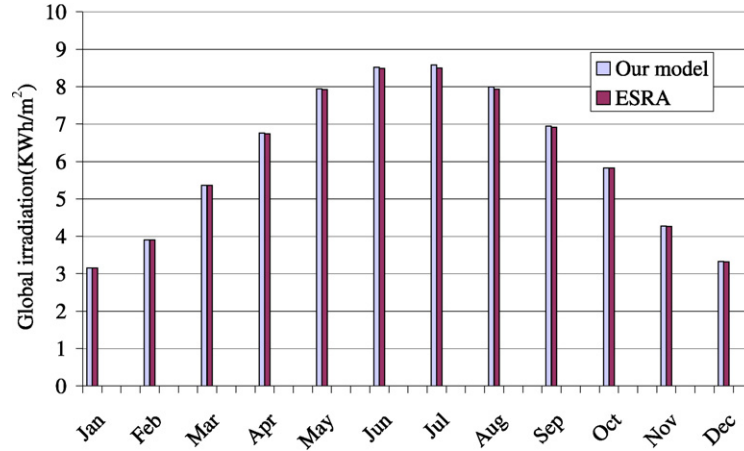
Fig. 4. Monthly global clear-sky *irradiation* for the year 2006, at the location of Malaga, Andalusia, Spain, calculated by our model (left column) and ESRA model (right column).

$$G_{ic} = \cos(\gamma_N) \cdot \text{val1} + \sin(\gamma_N) \cdot \text{val2} + \text{val3} \cdot F(\gamma_N)$$
$$+ \text{val4} + \sin(\gamma_N) \cdot \text{val5} + \rho_g(x, y) \cdot G_{hc} \cdot \text{val6}/360$$

　　　End For
　End For

For each specific height, horizon-point, and for each azimuthal sector, the algorithm calculates the *irradiation* as a sum of the corresponding terms from the arrays N_1, N_2, N_3, N_4, and N_5. Graphically, it consists of a sweeping of the energy-map represented in Fig. 3 by adding the terms that intersect the horizon curve. Notice that there is a different map for each class of energy (or term) and each z-level.

A comparison between the monthly global clear-sky *irradiation* calculated by our model and the values obtained by ESRA model [6] in the heterogeneous terrain of Malaga, as illustrated in Fig. 4, shows that they are actually very similar. The used monthly mean values of the Linke turbidity factor, T_{LK}, have been obtained from SODA database [12].

For a 1000×1000 points grid of resolution 10×10 m^2, an angular precision of one degree (i.e., sun elevation, sun azimuth, terrain aspect, and terrain slope precision equaling one degree) and five height-steps of 100 meters, typical execution time of this stage takes about 10 seconds. When the precision of the azimuth is reduced to 2 or 4 degrees, both memory usage and runtime are reduced to the same factor producing only slight changes in the results.

3.6. Real-sky irradiation

The proposed algorithm can be easily extended to compute the global *irradiation* under overcast conditions on horizontal and inclined surfaces. On *horizontal surfaces*, the global *irradiation* under real-sky conditions, G_h, is obtained by multiplying the global *irradiation* under clear-sky, G_{hc}, by the filtering factor, called the clear-sky index k_c [11,16,18]:

$$G_h = k_c \cdot G_{hc}. \tag{11}$$

The index k_c mainly represents the attenuation due to clouds and depends on the geographical coordinates of the considered horizontal plane [16–18]. For a set of meteorological stations,

the index k_c can be calculated as the ratio between the measured global *irradiation*, G_{hs}, and the theoretical values of the global clear-sky *irradiation*, G_{hc} [4]:

$$k_c = G_{hs}/G_{hc}. \tag{12}$$

For *inclined surfaces*, the clear-sky index, k_c, is computed separately for direct and diffuse components [4]:

$$k_c^b = B_h/B_{hc},$$
$$k_c^d = D_h/D_{hc}.$$

The values of the beam and diffuse components of the clear-sky index can be calculated using empirical equations [6,19] or using measured climatological data [4]; afterwards the corresponding raster maps of k_c^b and k_c^d can be calculated by applying a spatial interpolation [4]. Our model can easily use these raster maps when available to compute the real-sky global *irradiance/irradiation*. In particular, k_c^b and k_c^d are considered in the terms: T_1, T_2, T_3, T_4 and T_5 as follows:

$$T_1 = \cos(\gamma_N) \cdot \sum_{h_0=hor}^{90°} \sum_{m=m_i}^{m_e} \sin(h_0) \cdot K_b$$
$$\cdot \left(k_c^b + \frac{k_c^d \cdot F_1 \cdot (1 - \lambda_{twi})}{\sin(h_0)}\right) \cdot \sum_{k=1}^{n_{h,A_0}} \varepsilon,$$

$$T_2 = \cos(A_{LN}) \cdot \sin(\gamma_N) \cdot \sum_{h_0=hor}^{90°} \sum_{m=m_i}^{m_e} \cos(h_0) \cdot K_b$$
$$\cdot \left(k_c^b + \frac{k_c^d \cdot F_1 \cdot (1 - \lambda_{twi})}{\sin(h_0)}\right) \cdot \sum_{k=1}^{n_{h,A_0}} \varepsilon,$$

$$T_3 = F(\gamma_N, 1) \cdot \sum_{h_0=0}^{hor} F_d(h_0) \sum_{m=m_i}^{m_e} k_c^d \cdot T_n(m) \cdot \sum_{k=1}^{n_{h,A_0}} \varepsilon,$$

$$T_4 = \sum_{h_0=hor}^{90°} \cdot \sum_{m=m_i}^{m_e} k_c^d \cdot F(\gamma_N, 0) \cdot F_1 \cdot (1 - k_b) \cdot \sum_{k=1}^{n_{h,A_0}} \varepsilon,$$

Table 1
Selected cases for performance evaluation

	DEM size	Irradiation duration	Max height	Ground shadowing	Horizon shadowing
Case A	602×412	one year	500 m	included	–
Case B	602×412	one day	500 m	included	included
Case C	1000×1000	one year	200 m	included	–
Case D	1000×1000	one year	2000 m	included	included
Case E	1000×1000	one year	800 m	included	included

$$T_5 = \sin(\gamma_N) \cdot \cos(A_{LN}) \cdot \sum_{h_0=hor}^{5.7} \sum_{m=m_i}^{m_e} k_c^d$$

$$\cdot \frac{F_1 \cdot K_b}{0.1 - 0.008 \cdot h_0} \cdot \sum_{k=1}^{n_{h,A_0}} \varepsilon.$$

4. Computational and numerical results

Several analyses of the computational and numerical results are presented in this section. All results correspond to the portable implementation of the proposed model using C++ programming language. Parallel computing based on threads has been introduced into the code to better exploit current systems such as those based on multi-core processor technology in addition to shared memory architectures.

4.1. Computational cost independent on time-interval

An evaluation of the impact of: (1) the *irradiation* duration, (2) terrain irregularity, and (3) horizon shadowing, on the performance of each stage of the model is presented in Fig. 5. Five cases, of different degrees of irregularity, and *irradiation* duration have been considered as shown in Table 1.

- Case A: one year *irradiation* on a hilly terrain of size 602×412 cells, including ground shadowing only.
- Case B: One day *irradiation* on the same DEM as case A, including horizon shadowing.
- Case C: One year *irradiation* in a plain terrain of size 1000×1000 cells, with altitude changes inferior to 200 m, including ground shadowing only.
- Case D: One year *irradiation* in a 1000×1000 points grid with a large variation in height (maximum height difference of about 2000 m) including horizon shadowing.
- Case E: One year *irradiation* in a hilly terrain of size 1000×1000 cells and a maximum height of 800 m, including horizon shadowing.

Stage 1 runtime depends only on the *irradiation* time length and represents only 3.75% of the total cost. The computational cost of Stage 2 is similar for a one-day and one-year time-interval showing a slight increase when the number of the height-steps increases (see case D); this can be explained by the increase of the z-dimension of the matrices N_i which also implies further calculation. Stage 3 cost is similar for all considered cases. In addition to the increase due to the inclusion of the horizon shadowing, the runtime of the main loop increases substantially when the number of the height-steps increases.
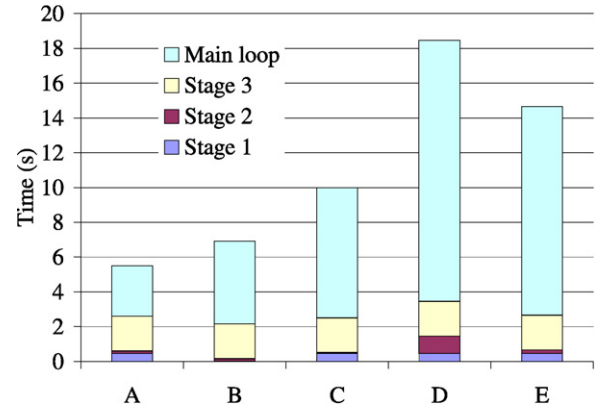

Fig. 5. Computational times of the stages: 1, 2, 3 and the main loop (described in Section 3.5) for the cases: A, B, C, D and E described in Table 1.

Summarizing, the computational cost of our model is almost independent on the *irradiation* time-interval; however, it is especially sensitive to the irregularity of the site and to the inclusion of horizon shadowing.

The computation of the *irradiation* on the DEM of Andalusia, of size 52000×32000 cells and resolution 10×10 m^2 [13], has been performed separately for 1664 tiles of 1000×1000 cells, consider Fig. 6. The runtime of the three preprocessing stages (described in Section 3) represents 90–95% of the total runtime. This cost can be reduced if these stages are reused; in fact, they should only be recalculated if the differences in latitude and atmosphere turbidity are significant. For any desired time-interval, the calculation of global irradiation in Andalusia takes about four hours and less than one day for the whole of Spain. The final time can be twice or three times greater due to the time employed to load the DEM and save the results.

4.2. r.sun versus our model

The comparison between our model and r.sun implementation of the ESRA model under GRASS 6.2.2 [5], has been carried out on a single Intel Pentium D and without including terrain shadowing.

The numerical difference between the daily global clear-sky irradiation calculated by our model and r.sun, ΔIrradiation $= G_{ic}$(our model) $- G_{ic}$(r.sun), for the Julian day 2454371, on an heterogenous terrain is presented in Fig. 7. This difference is insignificant since its absolute value is always smaller than 50 W h/m^2 day, i.e., smaller than 1% of the total value of daily irradiation. Indeed, 80% of the considered grid points have a value of $|\Delta$Irradiation$|$ smaller than 20 W h/m^2; consider the fourth curve in Fig. 8. The variation of ΔIrradiation can be ex-
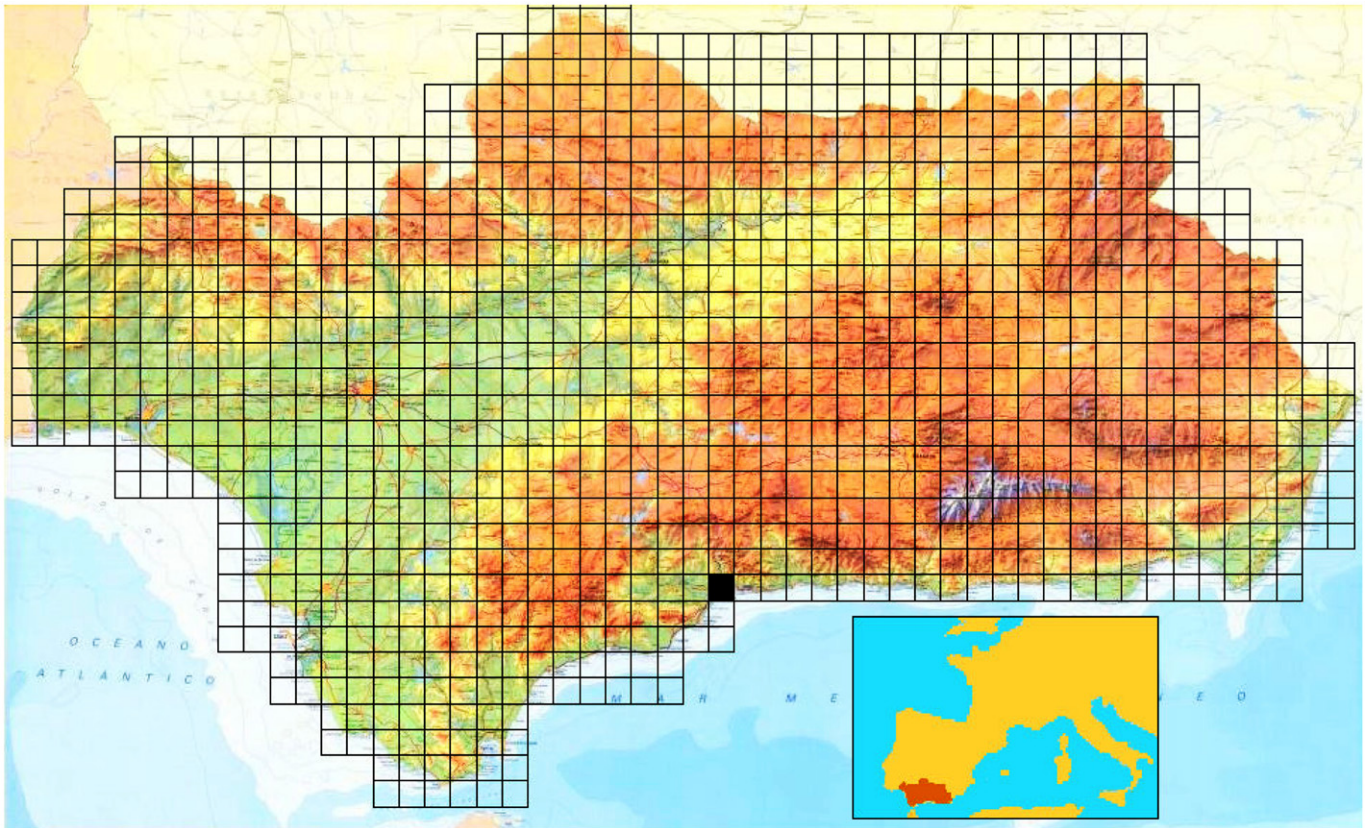
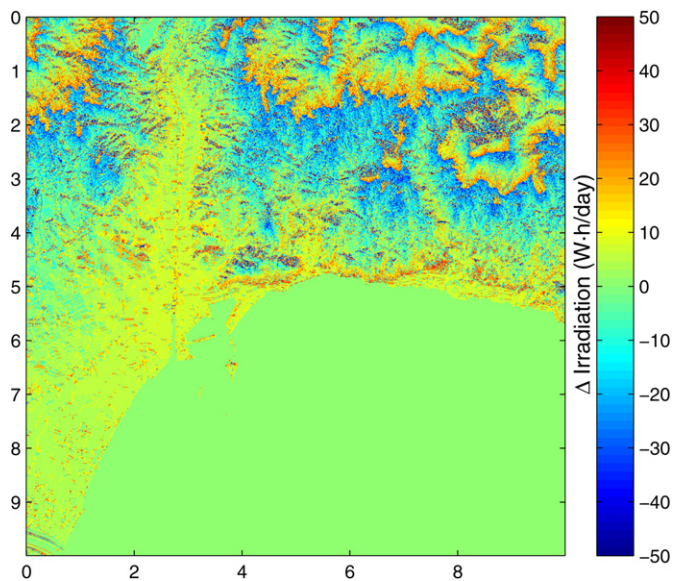Fig. 6. The black square shows the location of Malaga, Andalusia, Spain.

Fig. 7. Map of the numerical difference, ΔIrradiation (W h m^2 day), between daily global clear-sky irradiation calculated by our model and r.sun in the Julian day 2454371.

plained by its dependence on the heights z and the one degree discretization of the slope, aspect, and sky.

Calculating the daily global *irradiation* using r.sun on an irregular terrain of maximum height-difference equal to 800 m, of size 4500×5000 cells, using 15-min time-step, takes about 50 min. For the same conditions, our model takes 2.92 min;

about 17 times faster. As our model is independent of the simulation time length and step, it could be hundreds of times faster than r.sun for DEMs on the order of hundreds of millions of points. If the terrain shadowing is included, r.sun takes 250 min, while our model takes only 52.95 min; four times faster although in our model the horizon data are previously computed by an other application and can be reused in further computations of the same location [14].

5. Conclusions

Our model calculates the clear-sky *irradiation* on large territories considering that most computations can be independent on the terrain and on the simulated time-interval. In fact, it only considers a relatively reduced set of sun positions in the sky, and can also be easily extended to evaluate the *irradiation* on a reduced set of possible terrain orientations if no horizon shadowing is considered. In such a situation, the model would be almost independent on the terrain size and would only depend on the atmospheric conditions. Nevertheless, horizon shadowing should be considered in most situations, but even in this case, we have reduced the terrain size-dependent computations to a single loop in the azimuthal direction with seven floating operations in each sector. Irregular accesses to the matrices, due to the inherent irregularities of the horizons, will be analyzed in future work, as they become an important issue for the low ratio between flops and memory accesses.
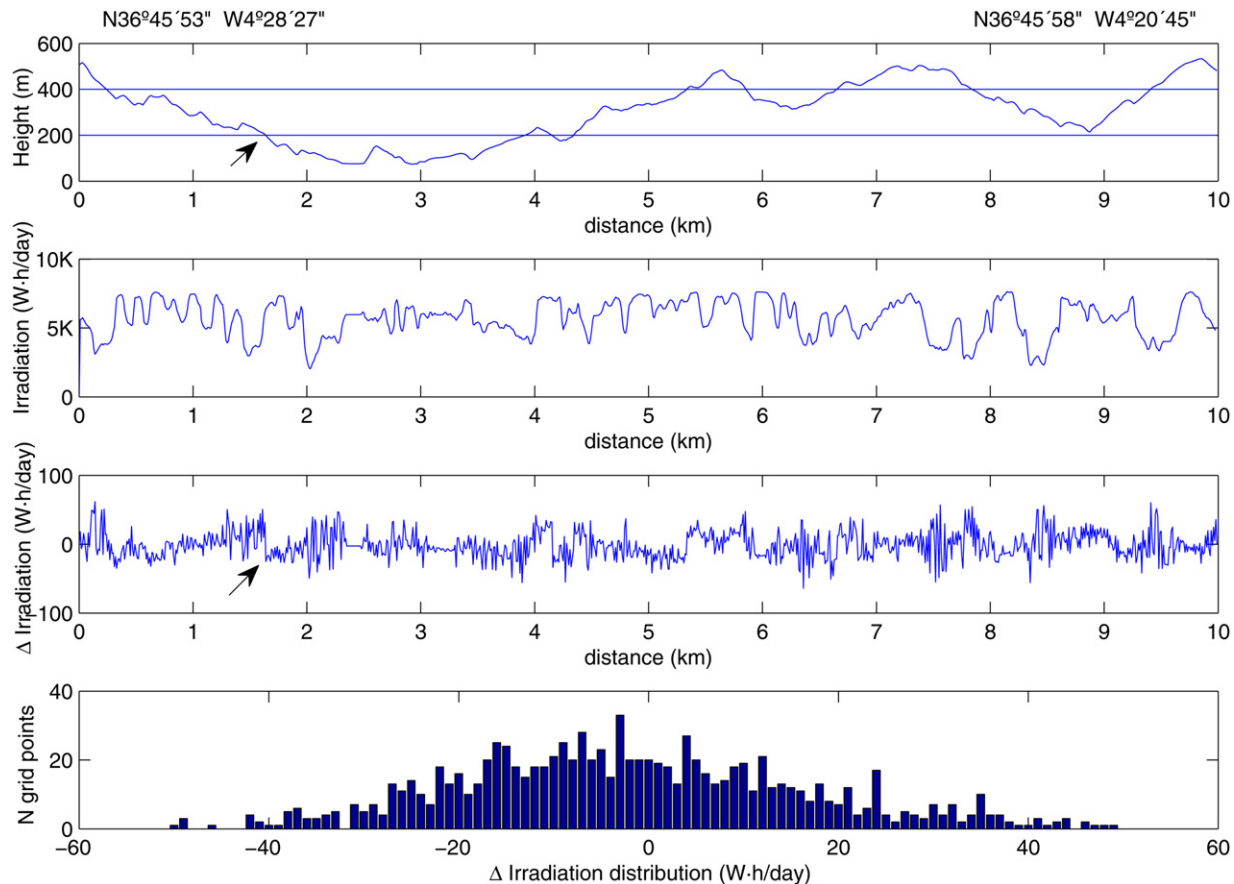
Fig. 8. From the top to the bottom, the first curve presents the heights, z, of the profile [N36°45′53″ W4°28′27″, N36°45′58″ W4°20′45″] form the DEM of Malaga. The second curve displays the corresponding daily global irradiation calculated by our model in the Julian day 2454371. The third curve displays the difference between daily global clear-sky irradiation calculated by our model and r.sun, ΔIrradiation. Finally, the fourth curve represents the distribution of ΔIrradiation in the considered profile.

Acknowledgements

References

[1] R. Dubayah, P.M. Rich, I. J. of Geographic Information Systems 9 (1995) 405.
[2] P. Fu, P.M. Rich, The solar analyst 1.0 User Manual, 2000.
[3] J.P. Wilson, J.C. Gallant (Eds.), Secondary Topographic Attributes, Terrain Analysis: Principles and Applications, John Wiley & Sons, New York, 2000.
[4] M. Suri, J. Hofierka, Trans. in GIS 8 (2004) 175.
[5] GRASS Development Team, Geographic Resources Analysis Support System (GRASS) Software, http://grass.itc.it, 2007.
[6] K. Scharmer, J. Greif (Eds.), Database and Exploitation Software, The European Solar Radiation Atlas, vol. 2, Les Presses de L'école des Mines, Paris, 2000.
[7] T. Muneer, in: Building Services Engineering Research & Technology, CIBSE, London, 1990, p. 153.
[8] T. Muneer, Solar Radiation and Daylight Models for Energy Efficient Design of Buildings, Architectural Press, Oxford, 1997.

[9] J.K. Page (Ed.), Prediction of Solar Radiation on Inclined Surfaces, D. Reidel Pub. Co., Dordrecht, 1986.
[10] C. Rigollier, O. Bauer, L. Wald, Solar Energy 68 (2000) 33.
[11] C. Rigollier, M. Lefevre, L. Wald, Heliosat Version 2: Integration and Exploitation of Networked Solar Radiation Databases for Environment Monitoring, Brussels, European Commission Project Nº IST-1999-122245 Report, http://www.soda-is.com, 2001.
[12] SODA: Services for Professionals in Solar Energy and Radiation, http://www.soda-is.com/eng/index.html.
[13] Digital elevation model of Andalusia, Relief and orography at 10 m, Junta de Andalusia, Spain, 2005.
[14] S. Tabik, J.M. Vías, E.L. Zapata, L.F. Romero, Lecture Notes in Comput. Sci. 4487 (2007) 54.
[15] A.J. Stewart, IEEE Trans. on Visualization and Comp. Graphics 4 (1998) 82.
[16] H.G. Beyer, C. Costanzo, D. Heinemann, Solar Energy 56 (1996) 207.
[17] H.G. Beyer, G. Czeplak, U. Terzenbach, L. Wald, Solar Energy 61 (1997) 389.
[18] A. Hammer, D. Heinemann, A. Westerhellweg, P. Ineichen, J.A. Oselth, A. Shartveit, D. Dumortier, M. Fontoynont, L. Wald, H.G. Beyer, C. Reise, L. Roche, J.L. Page, Derivation of daylight and solar *irradiance* data from satellite observations, in: Proc. of the Ninth Conf. on Satellite Meteorology and Oceanography, Paris, 1998, p. 747.
[19] F. Kasten, G. Czeplack, Solar Energy 24 (1980) 177.